Tb/s all-optical nonlinear switching using SOA based Mach-Zehnder interferometer

Y. Khorrami[a,*], V. Ahmadi[a] and M. Razaghi[b]

a. *Department of Electrical and Computer Engineering, Tarbiat Modares University, Tehran, P.O. Box 14115-143, Iran.*
b. *Department of Electrical and Computer Engineering, University of Kurdistan, Sanandaj, P.O. Box 416, Iran.*

Abstract. A new method for increasing the speed of all-optical Mach-Zehnder Interferometric (MZI) switching with a bulk Semiconductor Optical Amplifier (SOA), using chirped control signals, is suggested and theoretically analyzed. For 125fs input and chirped control pulses, we show acceleration of the gain recovery process using the cross phase modulation (XPM) effect. Our method depicts that Tb/s switching speeds, using bulk SOA-MZI with a proper Q-factor, is feasible. For the first time, we reach operation capability at 2Tb/s with a Q-factor of more than 10. The new scheme also improves the extinction and amplitude ratio of the output power, as well as increasing the contrast ratio of the switched signal. We use a finite difference beam propagation method for MZI analysis, taking into account all nonlinear effects of SOA, such as Group Velocity Dispersion (GVD), Kerr effect, Two Photon Absorption (TPA), Carrier Heating (CH) and Spectral Hole Burning (SHB).

1. Introduction

High-speed optical communication networks with terabit transmission capabilities attract much attention, in terms of high capability and flexibility in optical signal processing. Such ultrafast optical signal processing can be achieved using a Symmetric Mach Zehnder (SMZ) all optical switch family, including an original SMZ switch [1,2], a Delayed Interference Signal-wavelength Converter (DISC) [3], and a Polarization Discrimination SMZ (PD-SMZ) [4]. The Semiconductor Optical Amplifier (SOA) is a key element in many ultrafast switching schemes. The speed of switches based on SOA is limited, especially because of SOA carrier dynamics. To overcome this limitation, different approaches have been used. Wang et al. proposed and experimentally demonstrated a SOA based differential

scheme at 40 Gb/s [5]. Bischoff et al. suggested a new method using a XGM holding signal for increasing the speed of SOA-MZI converters to 160 Gb/s [6]. Nakamura et al. experimentally demonstrated a single channel OTDM, using a hybrid integrated SOA-MZI up to 168 GB/s [7-9]. Recently, Gutierrez suggested a new approach for all-optical signal processing using turbo-switched SOA-MZI at 160 Gb/s [10]. For bit rates higher than 168 Gb/s, data patterning effects are observed on the output signal, resulting in an increase in the probability of erroneous data detection. Repetition rates higher than 500 GB/s require a subpicosecond signal pulsewidth and the switching windows must approach the picosecond limit [1]. In these conditions, subpicosecond nonlinearities impose limitations on the switching structure. These limitations are attributed to inherent patterning effects associated with the gain recovery process in an SOA [6]. In this paper, we propose a new method for controlling the nonlinear phase difference between MZI arms, using chirped control pulses. As a result of the frequency chirp imposed on an optical pulse, its spectrum is consider-

*. *Corresponding author. Tel/Fax: +98 9190197109;*
   E-mail addresses: khorrami@isa.ir (Yaser Khorrami);
   v_ahmadi@modares.ac.ir (V. Ahmadi); m.razaghi@uok.ac.ir
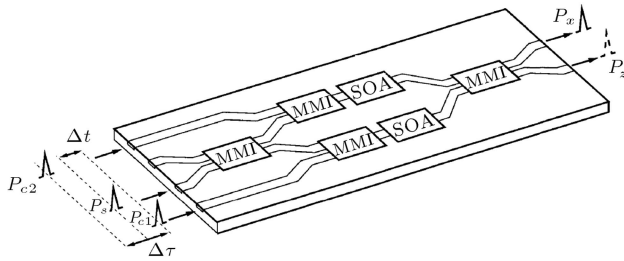   *(M. Razaghi)*

Figure 1. Structure of monolithically integrated MZI switch with two SOA's and four multimode interference couplers (MMIs). Signal (P_s) and control pulses (P_{c1}, P_{c2}) are used in the co-propagation arrangement.

ably broadened. On the other hand, unchirped pulses have the narrowest spectrum and are called transform-limited [11]. We show that the phase difference between MZI arms can be equalized uniformly due to spectrum broadening, compared with an unchirped condition, which provides a better pattern quality factor.

2. SOA-MZI switch

In our study, all optical switch modeling consists of a symmetric MZI with two SOA located in the same relative position of each arm, as shown in Figure 1.

The data signal enters the structure and splits symmetrically into each arm by the first multimode interference coupler (MMI). Two further control signals also are launched to each SOA via second and third couplers. The mechanism of switching is based on a time differential between control pulses, so that the data signal is injected between two control pulses. Control 1, as shown in Figure 1, is presented in the lower arm and changes the refractive index of the lower SOA before the signal pulse enters. Control 2 is injected to the upper arm after the data signal and saturates the upper SOA. In the switched state, the control pulse, P_{c1}, saturates the lower SOA, inducing a phase shift of $\Delta\varphi_{NL}$ between two arms, and a switched data signal from bar ($P_{\text{out}}^{=}$) to cross ($P_{\text{out}}^{\times}$) output port.

Control pulse, P_{c2}, switches back the SOA-MZI from constructive to destructive interference and so resets the switch for the next set of pulses that arrive. Output power can be written as [1]:

$$P_{\text{out}}^{=} = \frac{P_{\text{in}}}{8}\left\{G_1 + G_2 - 2\sqrt{G_1 G_2}\cos(\Delta\varphi_1 - \Delta\varphi_2)\right\},\tag{1}$$

$$P_{\text{out}}^{\times} = \frac{P_{\text{in}}}{8}\left\{G_1 + G_2 + 2\sqrt{G_1 G_2}\cos(\Delta\varphi_1 - \Delta\varphi_2)\right\},\tag{2}$$

$$\Delta\varphi_{NL}(t) = \Delta\varphi_1(t) - \Delta\varphi_2(t) = -(\alpha/2)\ln(G_2/G_1).\tag{3}$$

$P_{\text{in}}(t)$ is input power and $G_1(t)$, $\Delta\varphi_1$, $G_2(t)$ and $\Delta\varphi_2$ are the gain and phase differences of SOA1 and

SOA2, respectively. $\Delta\varphi_{NL}$ is the total phase difference accumulated by the optical signals given by Eq. (3). α is the linewidth enhancement factor associated with the gain changes due to carrier depletion and carrier heating. In the differential scheme, the switching window width is determined by the time-delay between the two control pulses [1] as:

$$T^{=} = \frac{1}{4}\left\{G_1 + G_2 - 2\sqrt{G_1 G_2}\cos(\Delta\varphi_1 - \Delta\varphi_2)\right\},\tag{4}$$

$$T^{\times} = \frac{1}{4}\left\{G_1 + G_2 + 2\sqrt{G_1 G_2}\cos(\Delta\varphi_1 - \Delta\varphi_2)\right\}.\tag{5}$$

3. Theoretical model

The following modified nonlinear Schrödinger equation [12-14] is used for the analysis of SOAs and the characteristics of the switching scheme:

$$\left[\frac{\partial}{\partial z} - \frac{i}{2}\beta_2\frac{\partial^2}{\partial\tau^2} + \frac{\gamma}{2} + \left(\frac{\gamma_2 P}{2} + ib_2\right)|V(\tau,z)|^2\right]V(\tau,z)$$

$$= \left\{\frac{1}{2}g_N(\tau)\left[\frac{1}{f(\tau)} + i\alpha_N\right]\right.$$

$$+ \frac{1}{2}\Delta g_T(\tau)(1 + i\alpha_T) - i\frac{1}{2}\frac{\partial g(\tau,\omega)}{\partial\omega}\bigg|_{\omega_0}\frac{\partial}{\partial\tau}$$

$$\left. - \frac{1}{4}\frac{\partial^2 g(\tau,\omega)}{\partial\omega^2}\bigg|_{\omega_0}\frac{\partial^2}{\partial\tau^2}\right\}V(\tau,z),\tag{6}$$

where:

$$g_N(\tau) = g_0\exp\left(-\frac{1}{W_s}\int_{-\infty}^{\tau}e^{-s/\tau_s}|V(s)|^2\,ds\right),\tag{7}$$

$$f(\tau) = 1 + \frac{1}{\tau_{shb}P_{shb}}\int_{-\infty}^{+\infty}u(s)e^{-s/\tau_{shb}}|V(\tau-s)|^2\,ds,\tag{8}$$

$$\Delta g_T(\tau)$$

$$= -h_1\int_{-\infty}^{+\infty}u(s)e^{-s/\tau_{ch}}\left(1 - e^{-s/\tau_{shb}}\right)|V(\tau-s)|^2\,ds,$$

$$-h_2\int_{-\infty}^{+\infty}u(s)e^{-s/\tau_{ch}}\left(1 - e^{-s/\tau_{shb}}\right)|V(\tau-s)|^4\,ds,\tag{9}$$

$$\frac{\partial g(\tau,\omega)}{\partial\omega}\bigg|_{\omega_0} = A_1 + B_1[g_0 - g(\tau,\omega_0)],\tag{10}$$

$$\frac{\partial^2 g(\tau,\omega)}{\partial \omega^2}\bigg|_{\omega_0} = A_2 + B_2[g_0 - g(\tau,\omega_0)], \qquad (11)$$

$$g(\tau,\omega_0) = g_N(\tau,\omega_0)/f(\tau) + \Delta g_T(\tau,\omega_0). \qquad (12)$$

A local time frame $\tau(= t - z/v_g)$ is introduced, which propagates with group velocity, v_g, at the center frequency of an optical pulse. The slowly varying envelope approximation is used in Eq. (4). Here, $V(\tau,z)$ is the time domain complex envelope function of an optical pulse, $|V(\tau,z)|^2$ corresponds to the optical power, β_2 is The Group Velocity Dispersion (GVD), γ is linear loss, γ_{2P} is the Two-Photon Absorption (TPA) coefficient, $b_2(= \omega_0 n_2/cA)$ is the instantaneous Self-Phase Modulation (SPM) term, due to the instantaneous nonlinear Kerr effect (n_2), $\omega_0(= 2\pi f_0)$ is the center angular frequency of the pulse, c is the velocity of light in a vacuum, A is the effective area of the active region, $g_N(\tau)$ is the saturated gain due to carrier depletion, g_0 is the linear gain, W_s is the saturation energy, τ_s is the carrier lifetime, $f(\tau)$ is the SHB function, P_{shb} is the SHB saturation power, τ_{shb} is the SHB relaxation time, α_N and α_T are the linewidth enhancement factors associated with gain changes, due to carrier depletion and Carrier Heating (CH), $\Delta g_T(\tau)$ is the resulting

gain change due to CH and TPA, $u(s)$ is the unit step function, τ_{CH} is the CH relaxation time, h_1 is the contribution of stimulated emission and free carrier absorption to CH gain reduction, h_2 is the contribution of TPA, A_1 and A_2 are the slope and curvature of linear gain at ω_0, and B_1 and B_2 are constants. The gain spectrum of an SOA can be approximated by the following second-order Taylor expansion in ω:

$$g(\tau,\omega) = g(\tau,\omega_0) + \Delta\omega\frac{\partial g(\tau,\omega)}{\partial \omega}\bigg|_{\omega_0}$$

$$+ \frac{(\Delta\omega)^2}{2}\frac{\partial^2 g(\tau,\omega)}{\partial \omega^2}\bigg|_{\omega_0}. \qquad (13)$$

The time derivative terms in the modified nonlinear Schrödinger equation are replaced with the central-difference approximation in order to solve the equation by the FD-BPM [12]. The parameters used in the simulation are listed in Table 1 [1,15].

4. Simulation results and discussion

Our numerical model is compared with Bischoff's results [16] in Figure 2. SOA's injection current

Table 1. The parameters used in simulation [1,15].

| Symbol	Quantity	Values (units)
L	SOA Length	500 μm
A	Effective area	5 μm^2
f_0	Center frequency of the pulse	193.5 THz
g_0	Linear gain	120 cm^{-1}
β_2	Group velocity dispersion	0.045 ps^{2}cm^{-1}
W_s	Saturation energy	10 pj
α_N	Linewidth enhancement factor due to the carrier depletion	7
α_T	Linewidth enhancement factor due to CH	1
h_1	The contribution of stimulated emission and free carrier absorption to the carrier heating gain reduction	0.3 cm^{-1}pj^{-1}
h_2	The contribution of TPA	300 fs cm^{-1}pj^{-2}
τ_s	Carrier lifetime	650 ps
τ_{CH}	Carrier heating relaxation time	800 fs
τ_{SHB}	SHB relaxation time	150 fs
P_{SHB}	SHB relaxation power	11.32 W
γ	Linear loss	15 cm^{-1}
n_2	Instantaneous nonlinear Kerr effect	-0.6 cm^{2}TW^{-1}
γ_{2P}	TPA coefficient	1.6 cm^{-1}W^{-1}
A_1		0.8 fs μm^{-1}
A_2	Parameters describing second order Taylor expansion of	-150 fs
B_1	the dynamically gain spectrum	-150 fs$^2\mu$m^{-1}
B_2		0 fs^2
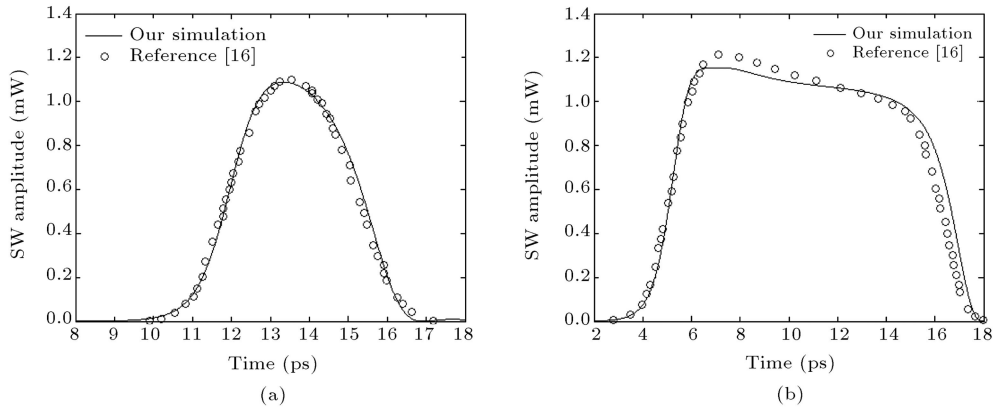
Figure 2. Switching Window (SW) amplitude versus time. SWs are shown for time-delay($\Delta\tau$) of (a) 4 ps and (b) 12 ps between the control pulses.

is 66.5mA and the input pulse Full Width at Half Maximum (FWHM) is 2 ps. The remaining parameters are the same as [16]. As shown in Figure 2, there is good agreement between our results and those in [16], according to two different time-delays, equal to 4ps and 12ps, in the switching window.

We consider the co-propagation state, which reveals a better performance regarding its small switching window and high ON/OFF ratio, while, in counter propagation, the switching window is larger [17,18]. Thus, for high speed applications, the co-propagation scheme is more reliable.

Based on the structure shown in Figure 1, Gaussian pulses with FWHM of 125 fs and pulse energy of 0.01 fJ, 18 fJ and 16 fJ are considered for signal and control pulses (P_s, P_{c1} and P_{c2}), respectively. Control pulses are launched with $\Delta\tau = 0.3$ ps delay to the switch.

Figure 3 depicts the time response of the integrated SOA MZI switch under unchirped and chirped control pulse conditions with 2 Tb/s input data signal and 0.5 Tb/s control pulse. Simulations are performed for two conditions of unchirped and chirped control pulses, but the input data pulse remains unchirped in all calculations. Figure 3(a) shows the MZI switching dynamics for a data pulse rate of 2Tb/s and a control pulse rate of 0.5 Tb/s, before and after each selected data pulse. In this case, data input pulse energy is chosen very low for preventing SOA's gain saturation by data pulse injection. Figure 3(b) and (c) show the switched output power for unchirped and chirped states, respectively.

Figure 3(b) shows the degradation of the switched pulse power because of the high carrier depletion rate of SOAs. Figure 3(c) shows the MZI output power for chirped Gaussian control pulses with a chirped factor of -5.

As observed, there is a considerable attenuation of peak patterns on the output switched power in Figure 3(b) as compared with Figure 3(c).
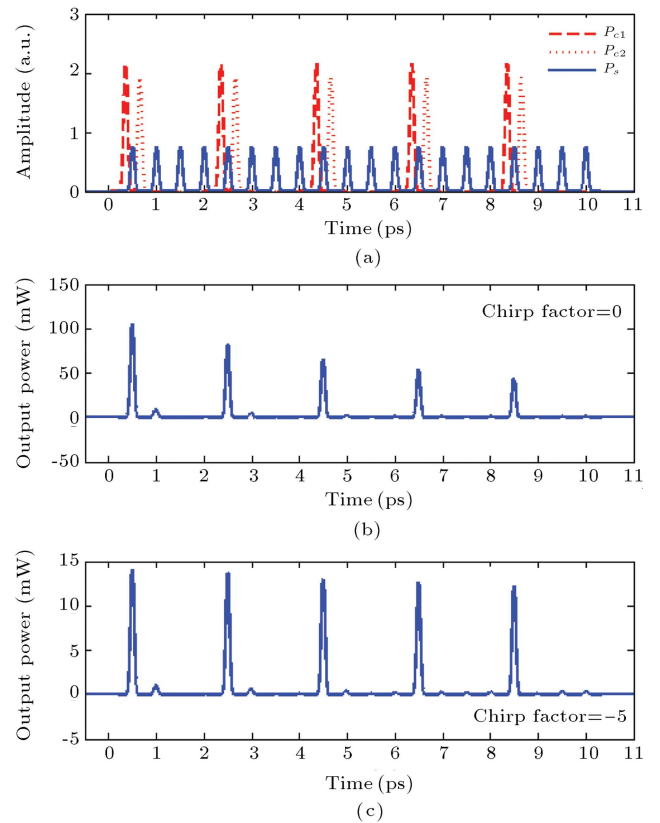

Figure 3. (a) 2 Tb/s input data signal and 0.5 Tb/s control pulses to the integrated SOA MZI switch. (b) Resulting MZI output power with unchirped control pulses, and (c) with chirped control pulses. Chirp factor is -5. Time delay between control pulses is 0.3 ps. The energy of input data pulse, control 1 and control 2 is 0.01 fJ, 18 fJ and 16 fJ, respectively.

To investigate this phenomenon, we analyze the SOA performance on each arm, as follows.

For Gaussian pulses with chirp factor of C, we use the following equation [11]:

$$A(0,t) = A_0 \exp\left(-\frac{1+iC}{2}\left(\frac{t}{T_0}\right)^2\right), \qquad (14)$$
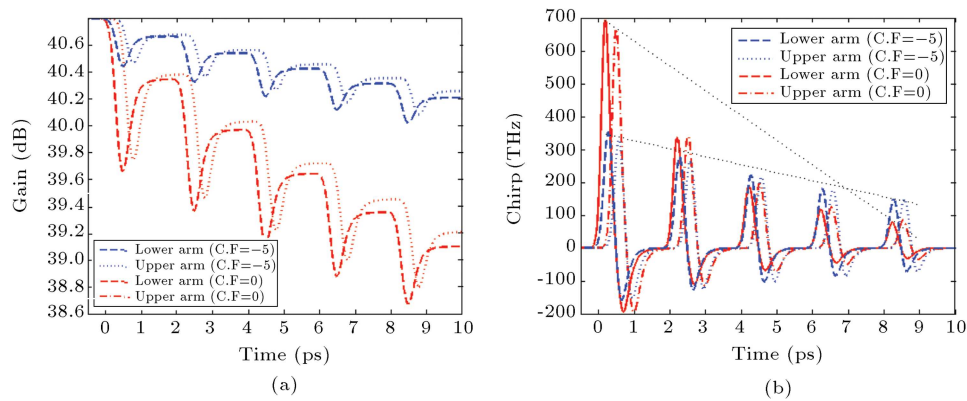
(a)

(b)

Figure 4. (a) Gain variation of each MZI arms with time. Upper arm has chirp factor of -5 and lower is unchirped. Carrier depletion rate reduces with adding negative chirp to control pulses. (b) Chirp variation of each MZI arms with time in two state of chirped and unchirped state for each control pulse.
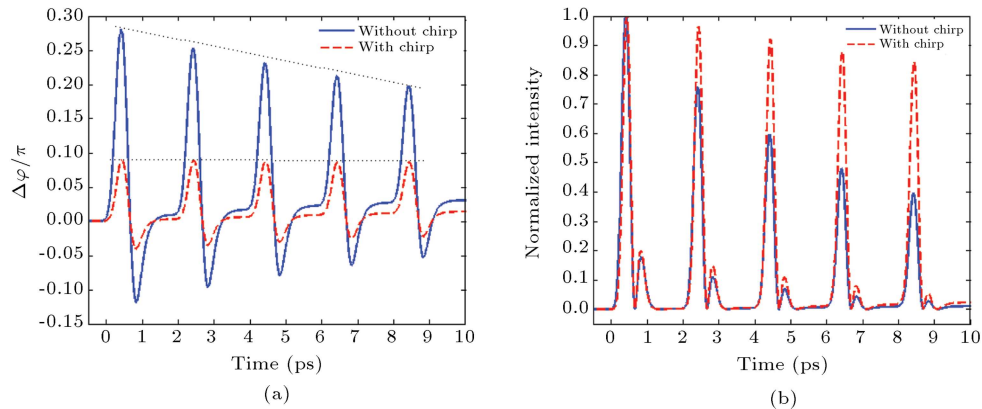

(a)

(b)

Figure 5. (a) Normalized phase difference between two arms of MZI. Phase variation is almost fixed for chirped state. (b) Variation of switching window with time. SW amplitude fluctuation is lower for chirped state.

where the parameter, C, represents the frequency chirp imposed on the pulse. A_0 is the peak amplitude and T_0 is the half-width at $1/e$ intensity point [11]. In all the following results, $C = -5$, is a fixed chirp factor.

Figure 4(a) shows the variation of MZI nonlinear gain in each arm. As shown, for the unchirped state, increasing gain recovery time after some switching processes leads to a patterning effect.

The chirped control pulses result in a lower amount of gain saturation, thus, reducing the output patterning effect compared to schemes with unchirped control pulses. The idea of using chirped control pulses temporarily equalizes the total power injected into the SOA's, thereby, reducing the patterning effect. As seen in Figure 4(a), injection of chirped control pulses reduces the SOA carrier depletion rate, resulting in a reduction of the gain (and also refractive index) changes induced by unchirped control pulses. It must be recognized that the recovery time of the SOAs takes place in a few ps and, therefore, the next bit cannot be processed until the SOAs are recovered. This poses a major limitation on application of a device without chirp injection.

Figure 4(b) shows the chirp variation of each MZI arm for chirped and unchirped control pulses. The results show the reduction of total chirp by each SOA in comparison to the unchirped state. Note that this reduction is noticeable for the first and second switched symbols, but for later ones, we have increments of chirp in both negative and positive chirp sections. This behavior obviously shows that for chirped control pulses, the slope of the chirp (shown by the dotted line in Figure 4(b)) is lower than that in the unchirped state. For more investigation, we calculated the phase difference and Switching Window (SW) amplitude variations versus the time in Figure 5.

Figure 5(a) shows the phase difference between two arms of MZI. Slower changes of phase difference on each switched symbol can reduce output patterning for the chirped state in comparison with the unchirped state. Figure 5(b) shows the amplitude of switching window as a function of time. In contrast, the fluctuation of SW amplitude for a chirped state is higher than for an unchirped state. As shown in Figure 4(b), in the presence of chirped control pulses, chirp variation becomes stable. As illustrated in Figure 5(a), the same
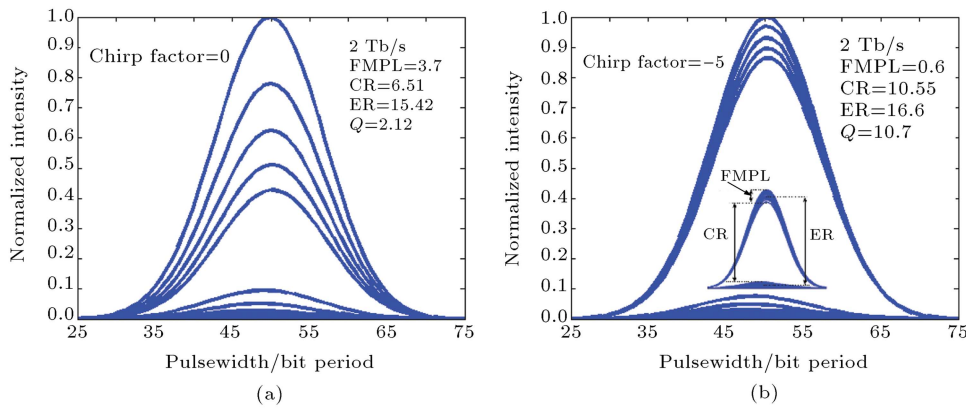
Figure 6. The optical eye diagram of MZI switch for 2Tb/s data rate for both (a) unchirped and (b) chirped states.

phenomena occurred for the differential phase in this case, which in turn leads to enhanced SW amplitude, as can be seen in Figure 5(b).

As a next step, we compare the eye diagram of each state. Figure 6(a) shows the eye diagram of the unchirped state, which is gradually closing due to the pattern effect, but which, for chirped control pulses, enhances system performance, based on Figure 6(b).

For performance evolution, we use four main parameters of switch over the output eye diagram. These are Fluctuation in the Mark Power Level (FMPL), Contrast Ratio (CR), Extinction Ratio (ER) and Quality factor (Q). These parameters are defined as [6,19-21]:

$$\text{FMPL} = \frac{P_{\max}^1}{P_{\min}^1}, \tag{15}$$

$$\text{CR} = \frac{P_{\text{mean}}^1}{P_{\text{mean}}^0}, \tag{16}$$

$$\text{ER} = \frac{P_{\min}^1}{P_{\max}^0}, \tag{17}$$

$$\text{Q} = \frac{P_{\text{mean}}^1 - P_{\text{mean}}^0}{\delta^1 + \delta^0}, \tag{18}$$

where $P_{\max}^1$, $P_{\min}^1$ and $P_{\max}^0$, $P_{\min}^0$ are the maximum and minimum values of the peak power of "1" and "0", respectively. P_{mean}^1 and P_{mean}^0 are the average power of output signals "1" and "0", and δ_1 and δ_2 are standard deviations of all "1" and "0". Figure 6(a) shows the unchirped state with FMPL, CR, ER and Q of 3.7, 6.51, 15.42 and 2.12, respectively. Figure 6(b) shows output switched signals with chirped control pulses ($C = -5$) and 0.6, 10.55, 16.6 and 10.7, as switch parameters equal to FMPL, CR, ER and Q, respectively. As seen, in the chirpy form, we have much better quality for switch factors. In this situation, the pattern effect becomes less and the eye pattern is clearly open with a Q of 10.7, in comparison with the unchirped state,

by a Q-factor of 2.12. Therefore, the recovery process is much faster for chirped states compared to case in which no chirp is applied to the switch.

In order to test the influence of the switching window width on the MZI switching behavior, we investigate the effect of time delay variation between two control pulses.

Figure 7 depicts the variation of four basic switch parameters (CR, ER, FMPL and Q-factor) with variation of delay time between two control pulses.

The curves are given for three different unsaturated gain ($G_0 = \exp(g_0 L)$) values equal to 22 dB, 24 dB and 26 dB in order to demonstrate the impact of linear gain g_0, and, equivalently, switch current on the output quality. The switch current for each SOA can be written as [22]:

$$I = \left(\frac{g_0}{\Gamma a N_0} + 1 \right) I_0, \tag{19}$$

where Γ is confinement factor, α is differential gain, and I_0 and N_0 are current and carrier density required for transparency, respectively. Taking G_0 instead of I gives freedom for experimental work, and one can change structural parameters to reach a specific g_0.

We obtain maximum CR, ER, Q and minimum FMPL for a time delay of around 0.2 ps, as shown in Figure 7. In Figure 7(a) and (b), we see same variations of CR and ER for every three amounts of G_0. Furthermore, as time delay decreases, our proposed scheme results are enhanced. Moreover, as depicted in Figure 7, for $\Delta \tau > 0.25$, CR and ER degrade when the time delay is increased, whilst the opposite occurs for the FMPL in Figure 7(c), so that FMPL has minimum points in the time delay of 0.4 when the unsaturated gains become 22 dB and 24 dB. FMPL curvature for $G_0 = 26$ dB has two relative minimum points in time delays of 0.15 ps and 0.82 ps in which 0.15 ps is the absolute minimum point. As seen, unsaturated gain variation does not imply sensitive differences on CR and ER, as shown in Figure 7(a) and (b).
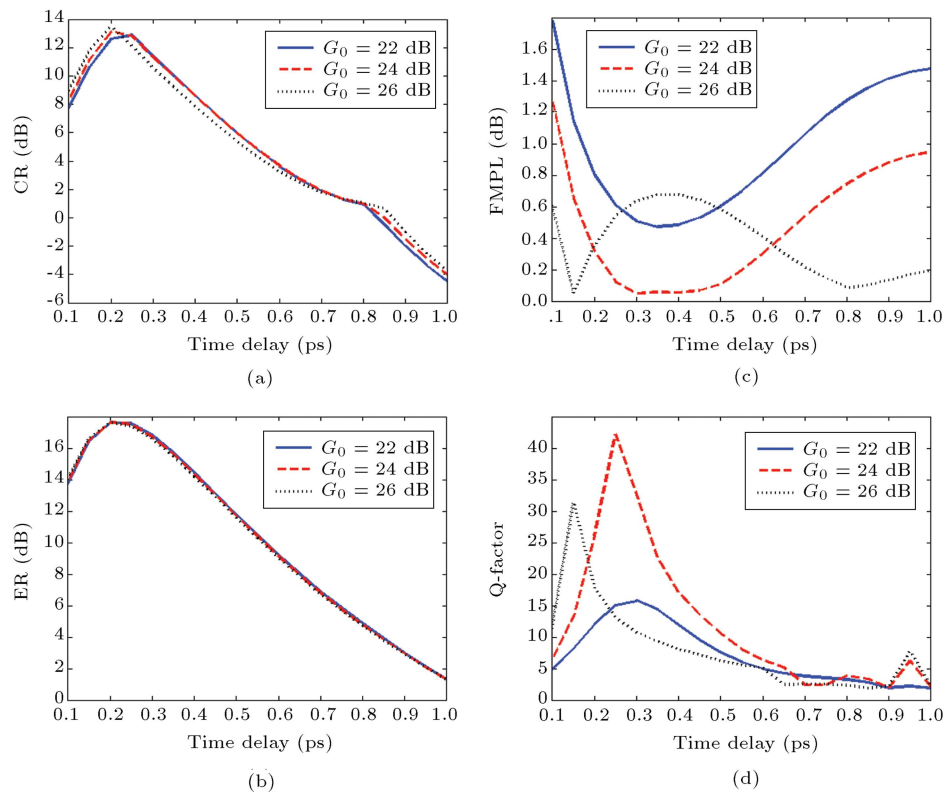
Figure 7. Variation of (a) CR, (b) ER, (c) FMPL and (d) Q-factor of switch with time delay between two control pulses for three different values of G_0 equal with 22, 24 and 26 dB.

The optimum Q-factor of the switch is shown for G_0 of 24 dB around 0.25 ps in Figure 7(d). Generally, larger time delay leads to lower Q-factor because of the decrease in the overlapping of two neighboring control pulses with the data pulse. Therefore, for larger time delay, the effect of chirp gradually decreases on the data switching mechanism. Figure 7 depicts that the best time delay is around 0.25 ps for G_0 of 24 dB.

Figure 8 displays the variation of switch parameters with the input data energy for different values of unsaturated gain. As before, we use chirped control pulses of $C = -5$, and 18 fJ and 16 fJ pulse energy for the first and second control pulses, respectively.

Figure 8(a) and (b) reveal that CR and ER degrade when the input data pulse energy is increased. Figure 8(c) shows that FMPL becomes larger as unsaturated gain increased. For $G_0 = 24$ dB, as illustrated in Figure 8(c) and (d), and input energies lower than 0.1 fJ, FMPL and Q-factor have minimum and maximum values, respectively. However, all switch parameters can be improved by decreasing the data pulse energy. For lower amounts of input data pulse energy, the effect of input data pulse energy on SOA saturation is eliminated and, therefore, the phase difference between the two arms is only adjusted with the energy of the chirped control pulses. Higher data energy imposes extra gain saturation on both MZI arms. Increases of input energy can saturate SOA

gain and this increases the unwanted switching rate for unexpected symbols. Thus, for higher values of input data pulse energy, we obtain far from ideal amounts of switch parameters, as seen in Figure 8(a) and (d).

To become clearer, we investigate chirp factor variation on switch output patterns. Figure 9 depicts the variation of four basic parameters (CR, ER, FMPL and Q-factor), with variations of the chirp factor of chirped control pulses, for three values of unsaturated gains of 22 dB, 24 dB and 26 dB. Figure 9 depicts that switch parameters are sensitive to the chirp of control pulses, so, an increase in the control chirp factor can slow down the carrier depletion rate in each arm and, therefore, gain recovery time decreases. Figure 9(a) and (b) show that for $G_0 = 22$ dB, there are better amounts of CR and ER. An increase of G_0 shows a higher rate of carrier depletion. Then, for lower values of G_0, as seen in Figure 9(a) and (d), better CR, ER, FMPL and Q-factor can be achieved not only in chirped, but also in unchirped approaches. Figure 9(d) depicts that the best Q-factor for positive chirp can be achieved in comparison with negative chirp.

Similarly, we can see this phenomenon in Figure 9(a) for positive chirp factors. The opening rate of the eye diagram for positive chirp is more than for the negative chirp, resulting in better values of Q-factor on positive chirp, as shown in Figure 9(d). By this illustration, we want to come back to Figure 4(b).
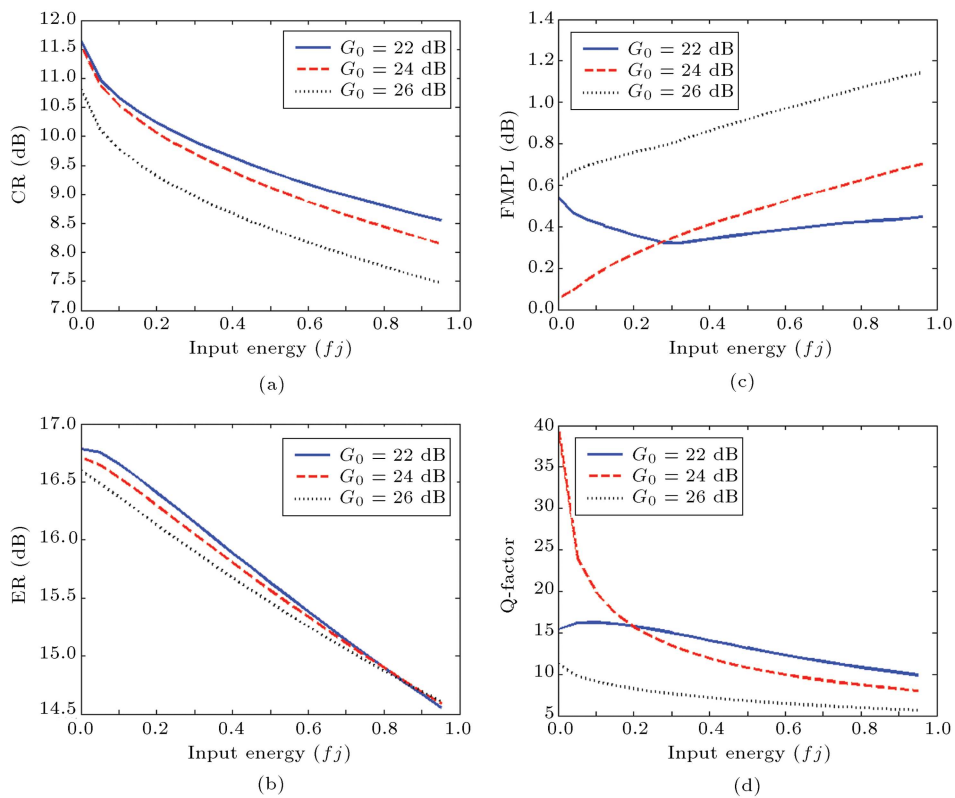
Figure 8. Variation of (a) CR, (b) ER, (c) FMPL, and (d) Q-factor with variation of input data energy for three different value of G_0 equal with 22, 24 and 26 dB.
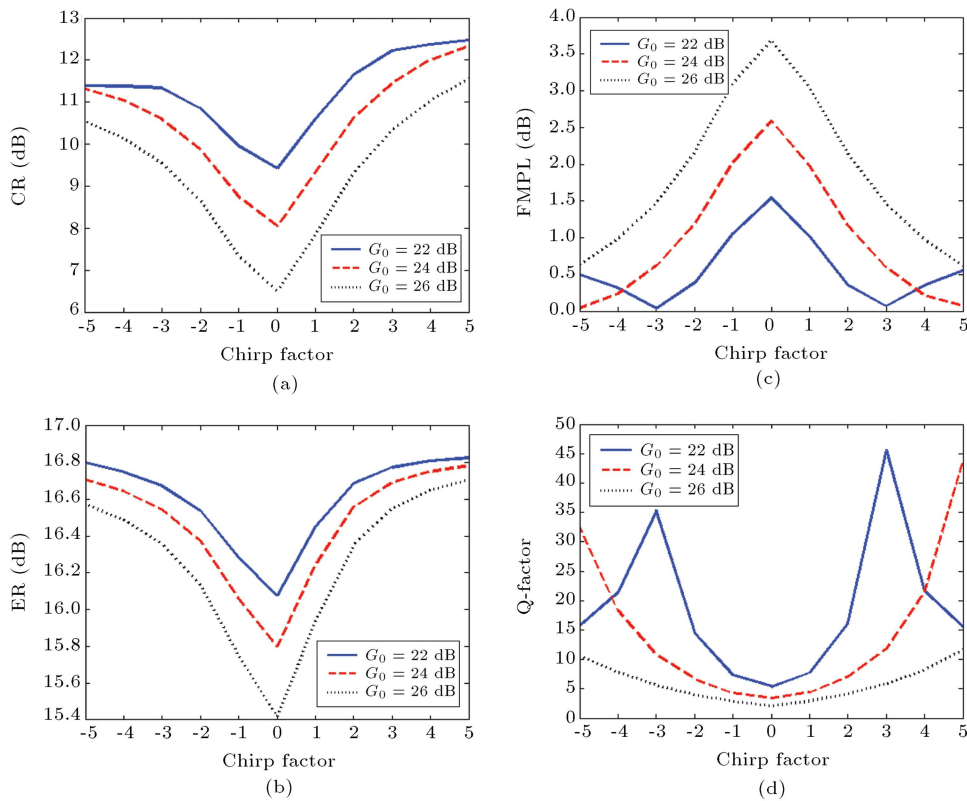

Figure 9. Variation of (a) CR, (b) ER, (c) FMPL, and (d) Q-factor with variation of chirp factor for three different value of G_0 equal with 22 dB, 24 dB and 26 dB. Input data energy, control 1 and 2 energies are 0.01 fJ, 18 fJ and 16 fJ, respectively. Time delay between two control pulses is 0.3 ps.

Figure 4(b) shows that for the negative chirp factor of control pulses, the slope of the dotted line is lower than the slope for the unchirped state. Similarly, for positive chirp factors, this slope becomes lower, in comparison with negative chirp factors. Therefore, more equalization can be found for the carrier depletion rate of positive chirp factors compared to negative ones. Figure 9(d) shows the best Q-factor for the chirp factor of +3 for $G_0 = 22$ dB. Furthermore, Figure 9(d) depicts that for positive chirps around +3, lower values of G_0 give a better Q-factor, whilst, in Figures 7(d) and 8(d), the best Q-factor takes place for higher amounts of unsaturated gain. This shows that chirp factor variation not only changes the Q-factor, but can also improve the output characteristics of the proposed scheme by selecting the proper unsaturated gain.

5. Conclusion

To achieve very high speed all-optical switching, for the first time, we use chirped control pulses as push-pull signals in a deferential symmetric MZI switching structure. Reduction of carrier depletion and gain saturation, and equalization of experienced chirp and phase differences in each MZI arm are the results of using chirped control pulses. Furthermore, this equalization is higher for positive chirp factors, further reducing the pattern effect in output switched pulses. Eye diagrams for two different chirped and unchirped states proved that the recovery process of each SOA can be improved for reaching quality factors higher than 10. We investigated the impact of data input energy, the time delay between two control pulses, and unsaturated gain, on basic parameters of the MZI switch. Our results show that femtosecond switching with higher efficiency is still possible using bulk SOAs.

Supper Gaussian pulses can be used for more investigation, because such pulses broaden more rapidly than Gaussian pulses. Therefore, super Gaussian chirped control pulses may be better candidates for future research on differential MZI switches.

Acknowledgement

References

1. Schreieck, R.P., Kwakernaak, M.H., Jackel, H. and Melchior, H. "All-optical switching at multi-100-Gb/s data rates with Mach-Zehnder interferometer switches", *IEEE J. of Quantum Electron*, **38**, pp. 1053-1061 (2002).

2. Nakamura, S., Ueno, Y. and Tajima, K. "Femtosecond switching with semiconductor-optical-amplifier-based symmetric Mach-Zehnder-type all-optical switch", *J. of Appl. Phys. Lett.*, **78**, pp. 3929-3931 (2001).

3. Ueno, Y., Nakamura, S., Tajima, K. and Kitamura, S. "3.8-THz wavelength conversion of picosecond pulse using a semiconductor delayed-interference signal-wavelength converter (DISC)", *IEEE Photon. Technol. Lett.*, **10**, pp. 346-348 (1998).

4. Tajima, K., Nakamura, S. and Sugimoto, Y. "Ultrafast polarization-discriminating Mach-Zehnder all-optical switch", *Appl. Phys. Lett.*, **67**, pp. 3709-3711 (1995).

5. Wang, Q., Zhu, G., Chen, H., Jaques, J., Leuthold, J., Piccirilli, A.B. and Dutta, N.K. "Study of all-optical XOR using Mach-Zehnder interferometer and differential scheme", *IEEE J. of Quantum Electron*, **40**, pp. 703-710 (2004).

6. Bischoff, S., Nielsen, M.L. and Mork, J. "Improving the all-optical response of SOAs using a modulated holding signal", *J. of Lightwave. Technol.*, **22**, pp. 1303-1308 (2004).

7. Nakamura, S., Ueno, Y., Tajima, K., Sasaki, J., Sugimoto, T., Kato, T., Shimoda, T., Itoh, M., Hatakeyama, H., Tamanuki, T. and Sasaki, T. "Demultiplexing of 168-Gb/s data pulses with a hybrid-integrated symmetric Mach-Zehnder all-optical switch", *IEEE Photon. Technol. Lett.*, **12**, pp. 425-427 (2000).

8. Nakamura, S., Ueno, Y. and Tajima, K. "168-Gb/s all-optical wavelength conversion with a symmetric-Mach-Zehnder-type switch", *IEEE Photon. Technol. Lett.*, **13**, pp. 1091-1093 (2001).

9. Tajima, K., Nakamura, S. and Ueno, Y. "Ultrafast all-optical signal processing with symmetric Mach-Zehnder type all-optical switches", *Optical and Quantum Electronics*, **33**, pp. 875-897 (2001).

10. Gutierrez, R. "Turbo-switched Mach-Zehnder interferometer performance as all-optical signal processing element at 160 Gb/s", *Optics Communications*, **282**, pp. 4345-4352 (2009).

11. Agrawal, G.P., *Fiber Optic Communication Systems*, Ed., 3th Edn., John Wiley Series in Microwave and Optical Engineering (2002).

12. Das, N.K., Yamayoshi, Y. and Kawaguchi, H. "Analysis of basic four-wave mixing characteristics in a semiconductor optical amplifier by the finite-difference beam propagation method", *IEEE J. of Quantum Electron*, **36**, p. 1184 (2000).

13. Das, N.K., Kawazoe, T., Yamayoshi, Y. and Kawaguchi, H. "Analysis of optical phase-conjugate characteristics of picosecond four-wave mixing signals in semiconductor optical amplifiers", *IEEE J. of Quantum Electron*, **37**, pp. 55-62 (2001).

14. Razaghi, M., Ahmadi, V. and Connelly, M. "Comprehensive finite-difference time-dependent beam propagation model of counterpropagating picosecond pulses in a semiconductor optical amplifier", *IEEE J. of Lightwave Technology*, **27**, pp. 3162-3174 (2009).

15. Kao, Y.H., Goltser, I.V., Jiang, M., Islam, M.N. and Raybon, G. "Gain dispersion induced subpicosecond pulse breakup in a fiber and semiconductor laser amplifier combined system", *Appl. Phys. Lett.*, **27**, pp. 4221-4223 (1996).

16. Bischoff, S., Buxens, A., Fischer, St., Dülk, M., Clausen, A.T., Poulsen, H.N. and Mørk, J. "Comparison of all-optical co- and counter-propagating high-speed signal processing in SOA-based Mach-Zehnder interferometers", *Optical and Quantum Electronics*, **33**, pp. 907-926 (2001).

17. Kang, K.I., Chang, T.G., Glesk, I. and Prucnal, P.R. "Comparison of Sagnac and Mach-Zehnder ultrafast all-optical interferometric switches based on a semiconductor resonant optical nonlinearity", *Appl. Optics*, **35**, pp. 417-426 (1996).

18. Toliver, P., Runser, R., Glesk, I. and Prucnal, P. "Comparison of Sagnac and Mach-Zehnder ultrafast all-optical interferometric switches based on a semiconductor resonant nonlinearity", *Conf. on Lasers and Electro Optics*, pp. 254-255 (2000).

19. Sun, H., Wang, Q., Dong, H., Chen, Z., Dutta, N.K., Jaques, J. and Piccirilli, A.B. "All-optical logic XOR gate at 80 Gb/s using SOA-MZI-DI", *IEEE J. of Quantum Electronics*, **42**, pp. 747-751(2006).

20. Taraphdar, C., Chattopadhyay, T. and Roy, J.N. "Mach-Zehnder interferometer-based all-optical reversible logic gate", *Optics and Laser Technology*, **42**, pp. 249-259 (2010).

21. Chattopadhyay, T. and Roy, J.N. "Semiconductor optical amplifier (SOA) - assisted Sagnac switch for designing of all-optical tri-state logic gates", *J. of Light and Electron Optics*, **12**, pp. 1073-1078 (2011).

22. Agrawal G.P. and Olsson, N.A. "Self-phase modulation and spectral broadening of optical pulses in semiconductor laser amplifiers", *IEEE J. of Quantum Electron*, **25**, pp. 2297-2306 (1989).

Biographies

Yaser Khorrami received his BS degree in Electronics Engineering from Kashan University, Kashan, Iran, in 2005, and an MS degree in Electrical Engineering from Tarbiat Modares University, Tehran, Iran, in 2011. He is, currently, working at the Iranian Space Agency (ISA), Tehran, Iran. His research interests include simulation and investigation of semiconductor optical amplifiers (SOA) in Mach Zehnder Interferometers.

He is also working on the Schrödinger equation for taking into account all nonlinear effects of the SOA-waveguide, such as Two Photon Absorption (TPA), Spectral Hole Burning (SHB), Carrier Heating (CH), Carrier Depletion (CD), Self-Phase Modulation (SPM), cross phase modulation (XPM), saturation energy effect and other effective parameters, like the Kerr effect. He has published and presented a number of papers at international conferences on Optics and Photonics.

Vahid Ahmadi received his BS degree in Electronics Engineering from Sharif University of Technology, Tehran, Iran, in 1986, an MS degree in Electrical Engineering from Tarbiat Modares University, Tehran, Iran, in 1990, and a PhD degree in Electrical Engineering from Kyoto University, Kyoto, Japan, in 1994. He is, currently, Professor in the Department of Electrical and Computer Engineering at the University of Tarbiat Modares, Tehran, Iran. He is a regular reviewer of several international technical journals and conference papers in the area of optical communications and photonic devices.

Mohammad Razaghi received a BS degree in Electronics Engineering from Razi University, Kermanshah, Iran, in 2001, and MS and PhD degrees in the same subject from Tarbiat Modares University, Tehran, Iran, in 2003 and 2009, respectively. He is, currently, Assistant Professor in the Department of Electrical and Computer Engineering at the University of Kurdistan, Sanandaj, Iran.

He is member of IEEE, and Deputy Chairman of the West Branch Iranian Association of Electrical and Electronics Engineers (IAEEE). He is a regular reviewer of several international technical journals and conference papers in the area of optical communications and photonic devices.